Surface Science 603 (2009) 2815–2819

Contents lists available at ScienceDirect

Surface Science

journal homepage: www.elsevier.com/locate/susc

Electrostatic field effect on molecular structures at metal surfaces

W. Guo [a], S.X. Du [a], Y.Y. Zhang [a], W.A. Hofer [b], C. Seidel [c], L.F. Chi [c], H. Fuchs [c], H.-J. Gao [a,*]

[a] Beijing National Laboratory of Condensed Matter Physics and Institute of Physics, Chinese Academy of Sciences, P.O. Box 603, Beijing 100190, China
[b] Surface Science Research Centre, University of Liverpool, Liverpool L69 3BX, UK
[c] Physics Institute, University of Münster, D-48149 Münster, Germany

ARTICLE INFO

Article history:
Received 30 March 2009
Accepted for publication 20 July 2009
Available online 29 July 2009

Keywords:
Scanning tunneling microscopy
Electrostatic field
Molecular structure transition

ABSTRACT

We report on the structural transitions of molecules on metal surfaces by external electrostatic field. An electrode–molecule–electrode model is considered to quantify the effect of electrostatic forces at the molecule–electrode interface. Within a quasi-parallel-plate capacitor approach, this model reveals how external electrostatic fields change the delicate balance between molecule–substrate and molecule–molecule interactions, leading to substantial changes in the molecular conformation. The predictions are validated by scanning tunneling microscopy (STM) observations of four different molecules and electrode facets. In addition, first-principles simulations verify the results of our model calculations.

1. Introduction

One of the key problems in the design and fabrication of molecular electronic devices [1] is understanding and controlling the conformation and structure of the molecules in an electrode–molecule–electrode system. It has been observed that a conformational change of molecules can cause dramatic changes of the physical properties and the corresponding device properties [2–9]. In a number of experiments it was demonstrated how the molecular conductance in organic thin films changes due to structural transitions, induced by electrostatic fields [10–19]. In one molecular device, Hu and coworkers have analyzed theoretically, how charge transport can be altered by a structural change at the molecule–electrode contacts [3]. Presently, it is of great interest for the wider community to estimate the level up to which electric fields can change the molecular structure at, e.g. metal surfaces. In principle, such a deeper understanding is most likely found in theoretical models, predicting molecular ordering at the atomic scale. However, precisely theoretical work has been somewhat lagging behind [20,21]. To date, no universal model exists, which could account in a comprehensive manner for the role electrostatic forces play in a molecule–electrode interface.

In this paper, we consider an electrode–molecule–electrode model to determine the effect of electrostatic forces at the molecule–electrode interface. Within a quasi-parallel-plate capacitor approach, the perturbation from the external electric field can be calculated and added to the free energy, obtained from first-principles electronic structure calculations. Qualitatively, the model reveals how external electric fields break the delicate balance between molecule–substrate and molecule–molecule interactions. We find that the molecular structures under an applied electrostatic field are controlled by the interplay of molecule–substrate interaction, intrinsic dipole moments, and the electric susceptibility of the molecular adlayer.

2. Model, theoretical considerations and experimental setup

It is well-known that molecules are susceptible to their chemical environment (substrate and other molecules) and external electric fields. They all contribute to the total energy (E_{total}) of the system. To investigate the effect of electrostatic field ($\vec{E}_e$) in the molecule–electrode interface, we compare the effects of electric fields to the energy gain when the charge redistribution occurs, and the interaction between the charge distribution and the electrostatic field. We regard the electrode–molecule–electrode system as a quasi-parallel-plate capacitor, which has been used in the past [22–25]. Then the total energy of the system can be written as:

$$E_{total} = E^0_{total} + \frac{1}{2}CU^2 + \int \rho(r)\varphi_e(r)d^3r \quad (1)$$

Here, C is the capacitance of the electrode–molecule–electrode system, U is the electric potential difference between the two electrodes, $\rho(r)$ is the charge density between the electrodes, and $\varphi_e(r)$ is the potential at position r. The second part in Eq. (1) is defined as charging energy which comes from the energy gain when the capacitor is charged. The third part in Eq. (1) can be rewritten in the multipole expansion:

* Corresponding author.
E-mail address: hjgao@iphy.ac.cn (H.-J. Gao).

0039-6028/$ - see front matter © 2009 Elsevier B.V. All rights reserved.
doi:10.1016/j.susc.2009.07.031

$$\int \rho(r)\varphi_e(r)\mathrm{d}^3r = Q\varphi_e(0) - \vec{\mu}\cdot\vec{E}_e - \frac{1}{6}\delta : \nabla\vec{E}_e \quad (2)$$

Here, Q is the total charge, $\vec{\mu}$ is the total dipole, and δ is the total quadrupole. Considering electroneutrality and neglecting the second order quadrupole, we may reduce Eq. (1) to:

$$E_{total} = E^0_{total} + \frac{1}{2}CU^2 - \vec{\mu}\cdot\vec{E}_e \quad (3)$$

Let us first discuss the quasi-parallel-plate capacitor. The electrode–molecule–electrode system is a suitable operation of an STM junction containing a metal substrate, a molecular interface, and a metallic tip (Fig. 1a). The reason that this approximation is justified lies in the fact that the radius for electrochemically etched W or Pt–Ir tips is generally about 10–30 nm [26]. Even in the high resolution STM images with sharper tips, the apex of the tip is mostly not smaller than the size of a molecule [27]. For a single molecule, the variation of electric field between STM tip and substrate with lateral distance is not dramatic, as established in model calculations on semiconductors [28]. To show that this is also the case for the metal–molecule–metal tip system, we consider a negatively charged W(100) tip (Fig. 1b). Here, the electrostatic potential indicates that the equipotential surface is quite close to a plane for distances higher than 4.7 Å. Contrary to the tunneling current, which is extremely sensitive to the distance, the electrostatic potential, as this simulation and previous work reveals, is far less volatile. In view of this feature it seems justified to mimic the tip potential by the electrostatic field to first order by two parallel metal plates.

Furthermore, the spacing between the tip and the substrate is at a nanometer scale. At this distance, the quantum capacitance is similar to the classical one only with little deviation in the absolute values [22,29]. Thus, it is a reasonable approximation to treat the capacitance using the classical Equation for the involved spacing of ~6 Å. In this distance range, which we are interested in, the total energy change induced by the external electric field can thus be written as:

$$\Delta E = \frac{1}{2}\varepsilon_0(1+\chi_e)Ad\cdot\left|\vec{E}_e\right|^2 - \vec{\mu}\cdot\vec{E}_e \quad (4)$$

where

$$\vec{\mu} = \vec{\mu}_0 + \chi_e\varepsilon_0 Ad\cdot\vec{E}_e \quad (5)$$

$$\left|\vec{E}_e\right| = \alpha(tip)\cdot\frac{U}{(1+\chi_e)d_v + d} \quad (6)$$

Here, $\vec{E}_e$ is the electric field of the molecular region, χ_e is the polarizability, ε_0 is the vacuum dielectric constant, A is the molecular effective area, representing the cross section of one unit cell for periodic structures, d is the effective height of the molecular layer, d_v is the height of vacuum region, and μ_0 is the dipole without electric field. The second part of Eq. (5) is the induced dipole moment in the volume Ad. In other words, the dielectric medium in the volume is polarized by the external electric field. Here we assume that the molecule is linearly polarized. $\alpha(tip)$ is a multiplier that describes the geometry-induced field enhancement. It can be approximately written as $Const/\left(r_{tip}\cdot h\cdot\sqrt{A}\right)$, where r_{tip} is the size of the tip apex (5 Å in our calculation), h the tip-sample distance, and $\sqrt{A}$ represents the lateral size of the adsorbate. According to the systems we simulated, it is found that the constant is universally about 805 Å^3. If $r_{tip}\cdot h\cdot\sqrt{A} > 805$ Å^3, α_{tip} can be simply chosen as unity. The internal interaction felt by molecules (molecule–substrate and molecule–molecule interaction) and the external electric field effect are the two crucial factors determining the molecular structure and orientation. In a conformational transition of an adsorbed molecule, ΔE acts as the activation energy. Comparing $|\Delta E|$ and the transition barrier $E_{barrier}$, we can therefore estimate how external electric fields will affect the molecular–electrode interface.

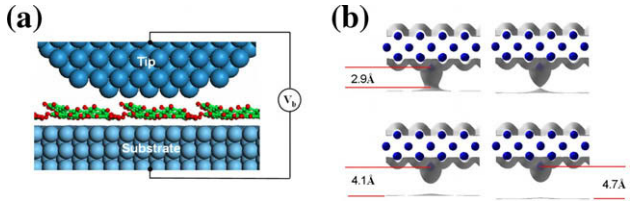

Fig. 1. (a) The model of the electrode–molecule–substrate system under a bias voltage. (b) A negative charged W(100) tip with a single atom apex (no molecules shown here) and the different equipotential planes. The supercell (12.7 Å × 12.7 Å × 41.1 Å) consists of 49 tungsten atoms. The electric potential in the supercell is obtained by first-principle calculations.

Our density functional theory (DFT) calculations were carried out with the Vienna *Ab-initio* Simulation Package (VASP). The Perdew–Wang generalized-gradient approximation (GGA) for exchange-correlation, ultrasoft pseudopotentials, and a plane-wave basis set as implemented in VASP code [30–32] were used. The supercell contained six layers of Ag atoms. The molecules were placed flat onto one side of the film with at least 12 Å of vacuum space. All atoms except the bottom two layers of the Ag film were fully relaxed until the net force on every atom was smaller than 0.015 eV/Å. After geometry optimization the total energy was obtained in the same energy cut-off and k-mesh.

To demonstrate the validity of the model, we studied experimental results on four different systems: (i) tetrabenz [a,c,h,j] anthracene (TBA) on Ag(110), (ii) Tb@C_{82}/octanethiol on Au(111) [16], (iii) polyvinylidene fluoride on graphite [17] and (iv) FAPPB(or PPB)-alkanethiol on Au(111) [19]. The substrates were chosen for the low adsorption energy of the molecules and, correspondingly, the importance of the balance between intermolecular and molecule–substrate interaction, which can be altered by external fields.

3. Model applications

3.1. TBA molecules on Ag(110) substrate

Conjugated molecule–metal interfaces are important systems in molecular electronics applications and have led to a substantial focus in research for decades [33]. In order to demonstrate the predictive power of the model, we therefore analyzed a conjugated planar system, TBA molecules on Ag(110) substrate. The detailed protocol can be found in Ref. [34–36]. The Ag(110) crystal was cleaned by standard sputtering with argon ions for 15 min at the pressure of 5×10^{-6} mbar followed by annealing at 350 °C for 3 min. After that, the cleaned Ag(110) surface was checked by LEED before deposition. Then the TBA molecules were evaporated from the sublimation cell onto the silver surface. The sample was transferred *in situ* into an Omicron STM operating at room temperature. First, we carried out experiments using an UHV-STM fitted with a molecular beam epitaxy (MBE) and low energy electron diffraction (LEED) apparatus. The background pressure of the chamber was better than 3×10^{-10} mbar. The molecular configurations under different electric fields are investigated based on the results from these two complementary surface analysis methods and DFT calculations. The LEED pattern indicates a unit cell containing two molecules. Subsequent STM results show a well-ordered dimer-like structure under positive bias voltage (see Fig. 2a). The dimer-like repeat unit is also evident in the line profile along a molecular row in Fig. 2a and the enlarged portion of the STM images in Fig. 2c. It is in good agreement with the LEED pattern.

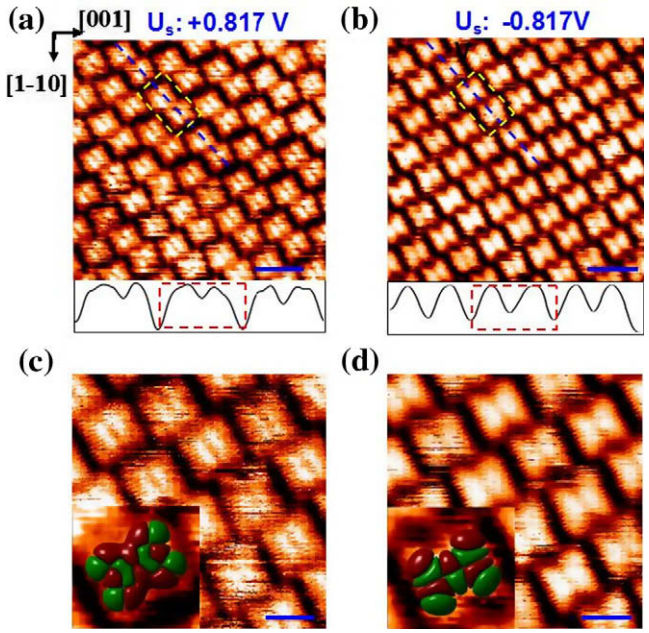

Fig. 2. (a,b) STM images (raw data) in the same region obtained with different polarity of the bias voltage. Scanning parameters: $I_t = 0.373$ nA, $U_s = +0.817$ V for (a) and −0.817 V for (b). The scale bars represent 2 nm. Substrate unit cell vectors are denoted as two green arrows. The two line profiles inserted at the right bottom are along the blue dashed lines in (a) and (b), respectively. (c,d) High resolution images of the same region. The scanning parameters are the same as (a,b). The scale bars represent 1 nm. Calculated probability density map of the LUMO and HOMO of the free TBA molecule are shown as insets in (c) and (d), respectively. (For interpretation of the references to color in this figure legend, the reader is referred to the web version of this article.)

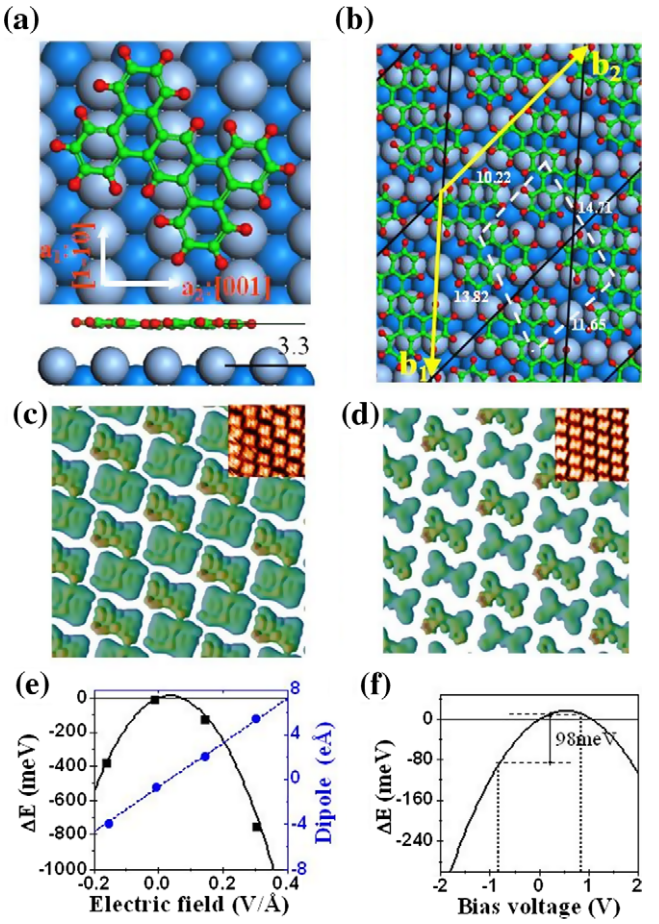

Fig. 3. The calculated molecular structures and simulated STM images. (a) Top and side views of single TBA molecule adsorption, the lattice of substrate is denoted with white arrows. (b) Top view of the dimer model (see text). The superlattice is denoted as black solid lines. White dashed-lines are used to illuminate the distances of neighboring molecules. The unit of distance is angstrom. (c,d) Simulated STM images of dimer structure under bias voltages of +0.817 V and −0.817 V, respectively. Color maps represent height in *Z*-direction. Insets are the images of experimental counterpart. (e) The total energy change (ΔE) and dipole moment induced by electric field effect as a function of the electric fields. The four black squares or blue circles are results from first-principles calculations and the solid and dashed lines are from fitted expressions. The error bar is represented with the size of the black squares and blue circles. (f) The total energy change (ΔE) with electric field effect as a function of the bias voltages with the parameters in our experiment ($\chi_e = 0.61$, $d = 2$ Å, $A = 295.1$ Å^2). The dashed line indicates the ±0.817 V in our experiment. (For interpretation of the references to color in this figure legend, the reader is referred to the web version of this article.)

However, in the same scanning area, when we change the polarity of the bias voltage, the dimer structure changes to a quasi-homogeneous structure shown in Fig. 2b and d. The self-assembled structure, it seems, is changed by the electric field. At this point, a question arises whether the difference at the reversed voltage biases is caused by a change of the molecular electronic structure or by a change of the molecular conformation (structure).

In order to clarify the origin of this bias-dependent image difference, we carried out DFT simulations of both a free molecule and the molecule–substrate system. By calculating different configurations of the TBA molecule adsorbed on Ag(1 1 0) with a large enough supercell, we obtained the most stable adsorption site and orientation of TBA/Ag(1 1 0). The most favorable adsorption site (Fig. 3a) is used to construct the supercell according to the LEED pattern. Two molecules are placed in one supercell each in its most favorable orientation. After geometry optimizations (Fig. 3b), the adsorption energy for this configuration is 316 MeV per molecule. We find that the distances between two neighboring molecules in the same supercell and the distance between two molecules in adjacent cells differ (white dashed lines in Fig. 3b), implying a dimer-like configuration. Simulated STM images on the adsorbed molecules (Fig. 3c and d) are compared with the experimental results (Fig. 2a and b). The partial charge densities within the interval from E_f to eV_{bias} agree very well with the STM images at positive and negative bias voltages. We find that the LUMO and HOMO structures of a single TBA molecule (see Fig. 2c and d) resemble the simulated STM images under positive and negative bias, respectively. At a positive bias, the simulated STM image (Fig. 3c) is more extended in X–Y plane than at a negative bias voltage (Fig. 3d). At a negative bias voltage, the image implies a quasi-homogeneous structure. The result at this point is unambiguous: the different appearance at a polarity change is due to the electronic structure of the system, and does not involve any structural changes of the molecule. Then the next question is can this behavior about the TBA/Ag(1 1 0) be predicted by our model?

If we apply an electric field [37] on the optimized dimer structure, the total energy changes $\Delta E = E_{total} - E^0_{total}$ and dipole moments of this configuration can be calculated depending on the intensity of the electric field. Here E_{total} is the total energy without electric field. We have calculated four points, −0.16 V/Å, 0 V/Å, 0.16 V/Å and 0.32 V/Å (Fig. 3e). The dipole moment changes linearly with the external electric field. However the curve for ΔE is quadratic. By calculating the slope of the blue dashed-line in Fig. 3e, the coefficient χ_e in Eq. (5) can be determined as 6.1 at =2 Å. Within the bias range from −0.817 to +0.817 V in our experiment, ΔE is 98 MeV (Fig. 3f). If the quasi-homogeneous STM image indicates a quasi-homogeneous molecular structure, the total energy is calculated to be 139 MeV/unit cell higher than the dimer structure. Since the transition barrier $E_{barrier}$ of these two structures is bigger than their energy difference, we conclude that the activa-

tion energy ΔE of the applied electric field cannot trigger structural transitions. However, if the molecule–substrate interaction is weak or the molecules have large dipole moments or intrinsic polarizability, the charging energy and dipole energy may well exceed the transition barrier. In such cases the competition between molecule–substrate interaction and interaction with the electric field will determine the systems behavior. The following three distinct examples for consequences of this effect.

3.2. Tb@C_{82}/octanethiol on Au(1 1 1)

For weak molecule–substrate interactions tiny energy changes due to external electric fields can change the molecular configuration. An example is Tb@C_{82}/octanethiol on an Au(1 1 1) substrate [16]. The octanethiol self-assembled monolayer (SAM) was inserted between Tb@C_{82} and the Au(1 1 1) substrate to reduce the interaction between molecule and metal substrate. It is then mainly van der Waals interaction between the molecules and the alkanethiol SAM. The Tb@C_{82} molecules rotate in an environment above 68 K, the energy threshold for the activation of the rotational mode is about 5.9 MeV. It was found that the molecular orientation can be switched, if the dipole moment of the Tb@C_{82} molecule is parallel to an external electric field with a sufficient high electrostatic energy (see upper panel in Fig. 4a). The *I–V* characteristic shows a hysteresis at 13 K due to the switching of the molecule. In an STM this transition occurs at a bias voltage of ±0.9 V. For the purpose of our model the dipole moment μ_0 of Tb@C_{82} molecule is 0.521 eÅ [16]. To take into account the double-barrier gap of the system, Eq. (6) was adapted as such:

$$\left|\vec{E}_e\right| = \alpha(tip)\cdot\frac{U}{(1+\chi_e)d_v + d + \frac{d_{oct}(1+\chi_e)}{1+\chi_{e-oct}}} \tag{7}$$

Because the molecule is not linearly polarized, we use two curves representing two initial states with opposite dipole moments (red and green lines in lower panel of Fig. 4a) . For a bias range from +2 V (step I) to −2 V (step IV) (see in lower panel of Fig. 4a), the applied bias voltage was changed gradually and then back to +2 V (step VII). The system reaches to its energy maximum at ±0.76 V (the two blue arrows), at about +6.3 MeV compared to zero bias voltage. Taking into account the weak interaction between Tb@C_{82} and octanethiol molecules as well as the thermal energy of only 1.1 MeV at 13 K, it can be expected that the external electric field will align the dipole moments of the molecules. In this case the Tb@C_{82} molecule changes its molecular orientation so that the molecular dipole moment is parallel to the external electric field at ±0.76 V. The switchings happen twice, the first is between step II and III, the second between V and VI, resulting in a hysteresis loop in the tunneling conductance. The prediction is in agreement with the experimental results. Thus it can be concluded that the weak interaction between Tb@C_{82} and the substrate, and the nonlinear polarization of Tb@C_{82} molecule, induced the switching of the molecular orientation, resulting in a distinct hysteresis loop.

3.3. P(VDF-TrFE) on graphite

Let us consider other cases whose interaction is the dominating part in the electric field effect. An example is the structural transition of a ferroelectric copolymer induced by a STM tip [17,18]. In this case, two layers of crystalline vinylidene fluoride (70%) with trifluoroethylene (30%) (P(VDF-TrFE)) copolymer were fabricated on a graphite substrate by the Langmuir–Blodgett (LB) technique at room temperature. By flipping the polarity of the tip bias, a structural transition and a switching of the dipole moment were achieved (see upper panel of Fig. 4b). The reversal of surface polarization is clearly demonstrated by the topographic images, showing an apparent local lattice distortion. It is very interesting that the structural transition only occurred in the flipping range of $0.1\ \text{V} \leqslant |V_{bias}| \leqslant 1.0\ \text{V}$, and it was most apparent at $|V_{bias}| \sim 0.57$ V. According to Ref. [38], the structural transition is directly related to rotation of the top layer molecules about the polymer chain axis. We calculated the total energy change with regard to the bias voltage with expression (4). Two curves are used to represent the two initial states with opposite dipole moment (red and green lines in lower panel of Fig. 4b). μ_0 of the monomer is about 0.3 eÅ [38]. We found that the energy difference ΔE between −1 V and +1 V is about 165 MeV, while ΔE the between −0.1 V and +0.1 V is about 17 MeV. FLAPW calculations on a two-layer polyvi-

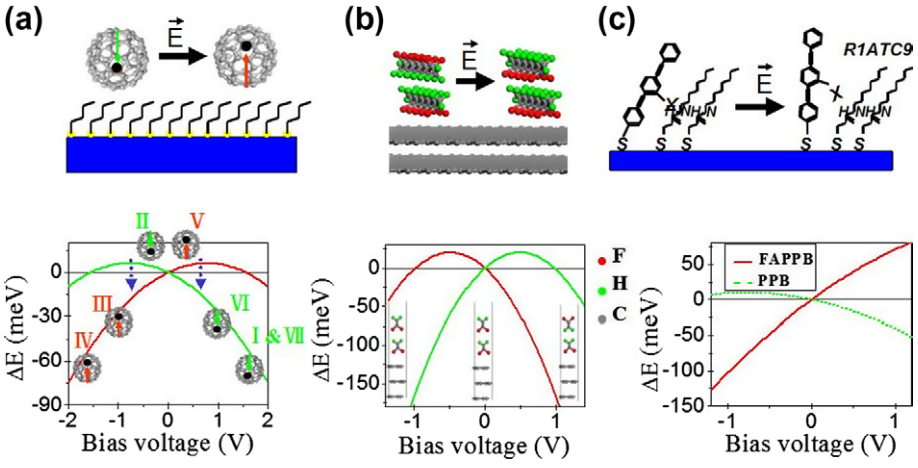

Fig. 4. Schematic view of the conformational changes of the models under electric field and the total energy change (ΔE) with electric field effect as a function of the bias voltages in references ([16] for (a), [17,18,38] for (b) and [19] for (c). Upper panel for the conformational changes; lower panel for the total energy changes.). The parameters are evaluated from the conditions in reference except for the polarizability, which is obtained by fitting. (a) The total energy change calculated for Tb@C_{82}/octanethiol on Au(1 1 1) with Eq. (4). ($\chi_e = 2.3, \chi_{e-oct} = 1.0$, $d_v = h = 6$ Å, $d = 6$ Å, $d_{oct} = 12$ Å, $A = 300$ Å^2). The numbers from I to VII indicate the sequences of bias voltages evolution in experiment. The red and green arrows indicate the direction of the dipole moment. The dotted arrows indicate that there are dipole moments switching at these bias voltages (see Fig. 4 in Ref. [16]). (b) The total energy change calculated with Eq. (4) with regard to P(VDF-TrFE). ($\chi_e = 10, d = 2.5$ Å, $d_v = h = 4$ Å, $A = 9$ Å^2). The sketch maps of P(VDF-TrFE) on graphite substrate are shown as insets. Red, green and gray balls denote fluorine, hydrogen and carbon atoms, respectively. The left one corresponds to the orientation with $V_{bias} < -1$ V, the right one with $V_{bias} > +1$ V, and the middle one with $|V_{bias}| < 0.1$ V (see Fig. 2 in Ref. [17]). (c) The total energy change calculated with Eq. (4) with regard to FAPPB and PPB molecules. ($\chi_e = 1.5, d = 10$ Å, $d_v = h = 6$ Å, $A = 100$ Å^2). (For interpretation of the references to color in this figure legend, the reader is referred to the web version of this article.)

nylidene fluoride slab showed that the energy difference between 0° and 90° is 27.2 MeV, while it is 131.3 MeV between 0° and 180° [38]. Thus we may conclude that for $|V_{bias}| = 0.1$ V the electric field will not trigger a visible rotation of the local dipole. In this case no structural transition appears (see the sketch in the middle inset of lower panel of Fig. 4b). For $|V_{bias}| = 1.0$ V, the dipole is rotated by 180° (the CF_2 switches from the bottom to the top as shown in left and right insets of Fig. 4b). This switching result in no lateral displacement, and no lattice shift appears in STM images. It explains why the lattice shift only occurred in the flipping range of $0.1\ \text{V} \leqslant |V_{bias}| \leqslant 1.0\ \text{V}$. In lower panel of Fig. 4b we show that the system reaches its energy maximum at about ±0.5 V, in accordance with the experimental observation that the lattice distortion was most apparent at $|V_{bias}| \sim 0.57$ V [18]. In this particular case the high polarizability of P(VDF-TrFE) is the crucial factor that controls the polymers orientation under external electric fields.

3.4. FAPPB or PPB/1ATC9 on Au(1 1 1)

As a final example we consider a monolayer of amide-containing alkanethiol (1ATC9) on an Au(1 1 1) substrate with oligo(phenylene ethynylene)s, FAPPB or PPB, embedded in it [19]. The STM image of FAPPB molecules changes when the bias voltage flips from −1 V to +1 V, or vice versa. It is attributed to a structural transition due to the formation and breaking of the hydrogen bonds (see upper panel of Fig. 4c). PPB molecules do not show bias voltage-dependent image changes. According to our model, the difference ΔE between −1 V and +1 V is about 176 MeV for FAPPB and 50 MeV for PPB molecules (see lower panel of Fig. 4c). The difference is due to the different dipole moments μ_0 of the two molecules, 0.812 eÅ for FAPPB and 0.229 eÅ for PPB [19], respectively. For FAPPB, the difference ΔE between −1 V and +1 V of 176 MeV, exceeds the energy barrier of the structural transition, the hydrogen bonding energy. Thus FAPPB molecules show a bias-dependent structural transition. For PPB molecules ΔE between −1 V and +1 V is 50 MeV, which will not exceed the barrier of the structural transition. Consequently, there is no bias-dependent structural transition. In this particular example the dipole moment is the crucial factor controlling the systems property under external electric fields.

4. Conclusions

By modeling the electrode–molecule–electrode system as a quasi-parallel-plate capacitor under small bias voltages, we are able to describe the total energy change and interfacial dipole moment under external electric fields. This quasi-parallel-plate capacitor model can be used to understand the effect of electrostatic forces in the molecule–electrode interface and to predict its effect. It also indicates that for molecules with large intrinsic dipole moment or large electric susceptibility, the polarity of electric fields between the two electrodes can cause substantial changes in the molecule/metal interface. By selecting a suitable combination of molecules and substrates, and by modulating experimental conditions like the bias voltage and the electrode–electrode distance, we can determine the molecular properties or change the molecular conformations. Due to a deeper understanding of bias-dependent molecular configurations the method should aid in designing and controlling devices at the molecular level, allowing a much more efficient direction of future research.

Acknowledgements

We thank L. Gao and J.T. Sun for technical assistance. This work is supported by the National Science Foundation of China (NSFC) (Grant No. 10774176), National "973" Projects of China (Grant Nos. 2006CB806202 and 2006CB921305), CAS, Shanghai Supercomputer Center and the Supercomputing Center, CNIC.

References

[1] H.B. Akkerman, P.W.M. Blom, D.M. de Leeuw, B. de Boer, Nature 441 (2006) 69.
[2] L. Venkataraman, J.E. Klare, C. Nuckolls, M.S. Hybertsen, M.L. Steigerwald, Nature 442 (2006) 904.
[3] Y.B. Hu, Y. Zhu, H.J. Gao, H. Guo, Phys. Rev. Lett. 95 (2005) 156803.
[4] F. Moresco, G. Meyer, K.-H. Rieder, H. Tang, A. Gourdon, C. Joachim, Phys. Rev. Lett. 86 (2001) 672.
[5] L.P. Ma, Y.L. Song, H.J. Gao, W.B. Zhao, H.Y. Chen, Z.Q. Xue, S.J. Pang, Appl. Phys. Lett. 69 (1996) 3752.
[6] S.X. Du, H.J. Gao, C. Seidel, L. Tsetseris, W. Ji, H. Kopf, L.F. Chi, H. Fuchs, S.J. Pennycook, S.T. Pantelides, Phys. Rev. Lett. 97 (15) (2006) 156105.
[7] H.J. Gao, K. Sohlberg, Z.Q. Xue, H.Y. Chen, S.M. Hou, L.P. Ma, X.W. Fang, S.J. Pang, S.J. Pennycook, Phys. Rev. Lett. 84 (2000) 1780.
[8] M. Feng, X. Guo, X. Lin, X. He, W. Ji, S.X. Du, D.Q. Zhang, D.B. Zhu, H.J. Gao, J. Am. Chem. Soc. 127 (2005) 15338.
[9] M. Feng, L. Gao, Z. Deng, W. Ji, X. Guo, S.X. Du, D.X. Shi, D.Q. Zhang, D.B. Zhu, H.J. Gao, J. Am. Chem. Soc. 129 (2007) 2204.
[10] Z.J. Donhauser, B.A. Mantooth, K.F. Kelly, L.A. Bumm, J.D. Monnell, J.J. Stapleton, D.J. Price, A.M. Rawlett, D.L. Allara, J.M. Tour, P.S. Weiss, Science 292 (2001) 2303.
[11] J. Lahann, S. Mitragotri, T.-N. Tran, H. Kaido, J. Sundaram, I.S. Choi, S. Hoffer, G.A. Somorjai, R. Langer, Science 299 (2003) 371.
[12] Q.-M. Xu, M.-J. Han, L.-J. Wan, C. Wang, C.-L. Bai, B. Dai, J.-L. Yang, Chem. Commun. (2003) 2874.
[13] G.-J. Su, H.-M. Zhang, L.-J. Wan, C.-L. Bai, T. Wandlowski, J. Phys. Chem. B 108 (2004) 1931.
[14] Y.-L. Yang, Q.-L. Chan, X.-J. Ma, K. Deng, Y.-T. Shen, X.-Z. Feng, C. Wang, Angew. Chem., Int. Ed. 45 (2006) 6889.
[15] X.H. Qiu, G.V. Nazin, W. Ho, Phys. Rev. Lett. 93 (2004) 196806.
[16] Y. Yasutake, Z. Shi, T. Okazaki, H. Shinohara, Y. Majima, NanoLetters 5 (2005) 1057.
[17] H. Qu, W. Yao, T. Garcia, J. Zhang, A.V. Sorokin, S. Ducharme, P.A. Dowben, V.M. Fridkin, Appl. Phys. Lett. 82 (2003) 4322.
[18] L. Cai, H. Qu, C. Lu, S. Ducharme, P.A. Dowben, J. Zhang, Phys. Rev. B 70 (2004) 155411.
[19] P.A. Lewis, C.E. Inman, F. Maya, J.M. Tour, J.E. Hutchison, P.S. Weiss, J. Am. Chem. Soc. 127 (2005) 17421.
[20] W.A. Hofer, Prog. Surf. Sci. 71 (2003) 147.
[21] K. Leung, S.B. Rempe, P.A. Schultz, E.M. Sproviero, V.S. Batista, M.E. Chandross, C.J. Medforth, J. Am. Chem. Soc. 128 (2006) 3659.
[22] J.G. Hou, B. Wang, J. Yang, X.R. Wang, H.Q. Wang, Q. Zhu, X. Xiao, Phys. Rev. Lett. 86 (2001) 5321.
[23] G.V. Nazin, S.W. Wu, W. Ho, PNAS 102 (2005) 8832.
[24] N.P. Guisinger, N.L. Yoder, M.C. Hersam, PNAS 102 (2005) 8838.
[25] R. Akiyama, T. Matsumoto, T. Kawai, Phys. Rev. B 62 (2000) 2034.
[26] C.J. Chen, Introduction to Scanning Tunneling Microscopy, second ed., Oxford University Press, New York, 2008.
[27] Y.L. Wang, H.J. Gao, H.M. Guo, H.W. Liu, I.G. Batyrev, W.E. McMahon, S.B. Zhang, Phys. Rev. B 70 (2004) 073312.
[28] K. Stokbro, Surf. Sci. 429 (1999) 327.
[29] M. Tanaka, Y. Gohda, S. Furuya, S. Watanabe, Jpn. J. Appl. Phys. 42 (2003) L766.
[30] J.P. Perdew, J.A. Chevary, S.H. Vosko, K.A. Jackson, M.R. Pederson, D.J. Singh, C. Fiolhais, Phys. Rev. B 46 (1992) 6671.
[31] G. Kresse, J. Furthmüller, Phys. Rev. B 54 (1996) 11169.
[32] G. Kresse, J. Hafner, Phys. Rev. B 47 (1993) 558.
[33] J.V. Barth, G. Costantini, K. Kern, Nature 437 (2005) 671.
[34] Y.L. Wang, W. Ji, D.X. Shi, S.X. Du, C. Seidel, Y.G. Ma, H.J. Gao, L.F. Chi, H. Fuchs, Phys. Rev. B 69 (2004) 075408.
[35] Z.H. Cheng, L. Gao, Z.T. Deng, Q. Liu, N. Jiang, X. Lin, X.B. He, S.X. Du, H.-J. Gao, J. Phys. Chem. C 111 (2007) 2656.
[36] L. Gao, W. Ji, Y.B. Hu, Z.H. Cheng, Z.T. Deng, Q. Liu, N. Jiang, X. Lin, W. Guo, S.X. Du, W.A. Hofer, X.C. Xie, H.-J. Gao, Phys. Rev. Lett. 99 (2007) 106402.
[37] P.J. Feibelman, Phys. Rev. B 64 (2001) 125403.
[38] C.-G. Duan, W.N. Mei, W.-G. Yin, J. Liu, J.R. Hardy, S. Ducharme, P.A. Dowben, Phys. Rev. B 69 (2004) 235106.